8th International Colloquium on Bluff Body Aerodynamics and Applications
Northeastern University, Boston, Massachusetts, USA
June 7 - 11, 2016
BBAA VIII

Experimental and numerical aerodynamic analysis of a concrete railway bridge in tandem arrangement with a truss road bridge

A. Zasso [a], D. Rocchi [b], T. Argentini [c], S. Giappino [d], T. Costantini [e]

[a] *Politecnico di Milano, Milan, Italy, alberto.zasso@polimi.it*
[b] *Politecnico di Milano, Milan, Italy, daniele.rocchi@polimi.com*
[c] *Politecnico di Milano, Milan, Italy, tommaso.argentini@polimi.it*
[d] *Politecnico di Milano, Milan, Italy, stefano.giappino@polimi.it*
[e] *Politecnico di Milano, Milan, Italy, t.costantini89@gmail.com*

SUMMARY:
An aerodynamic study of a tandem arrangement between two different bridge decks is presented in this paper. Wind tunnel tests on sectional were carried out to assess the dynamic performance of the deck of a new railway bridge, that is going to be built next to an existing roadway truss bridge. During wind tunnel tests two different concepts for the new deck were investigated: a standard bluff solution and a streamlined solution. The two solutions lead to very different aerodynamic behavior, both in stand-alone configuration and in tandem arrangement with the existing bridge. Steady and unsteady aerodynamic coefficients were measured on both the new bridge deck solutions in stand alone, upwind and downwind configurations. CFD 2D RANS simulations were used to have a better understanding of the aerodynamic interference effects.

Keywords: cable-stayed bridge, tandem arrangement, wind tunnel tests, CFD, RANS, Equivalent Porosity model

1. INTRODUCTION

Metro lines are growing faster and faster and more and more often lightweight metro trains are running on viaducts and bridges in the suburban areas. The railway infrastructure is expanding in region where the road traffic is already developed and usually the position of river or channel crossings are shared between road and railway traffic. New bridges or viaducts are built close to the existing road ones, because of the different requirements of the railway system, and bridges in tandem arrangement are becoming a widely adopted solution. Sometimes the distance of the new bridge from the existing one is so small that the decks aerodynamics cannot be considered as independent and specific investigations must be performed. In many cases the characteristics of two bridges are very different, as in the present study, since they belong to different ages and they are design after different requirements (pedestrian, road, railway or mixed traffic). For instance, in the presented research a new concrete railway bridge and an already existing steel truss road bridge are considered.

Railway concrete bridges with small spans usually have bluff sections and poor aerodynamic shapes. Their large mass and high natural frequencies help them to prevent aero-elastic problems when design wind speed are sufficiently low. In the study, the wind design speed (86 m/s) is high (tropical zone), and the bridge span (650 m) is long enough to ask for an aeroelastic investigation of the bridge behavior. Moreover, the small distance between the two decks, that are 10 m apart,

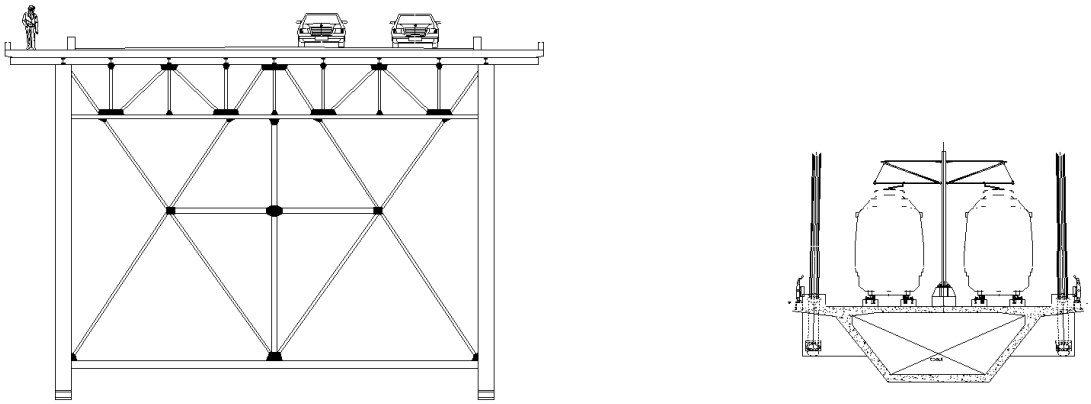

Figure 1. Existing roadway truss bridge and new railway cable stayed bridge

and relative position (decks are at different heights), ask also to analyses possible aerodynamic interactions.

This paper shows the results achieved through sectional wind tunnel studies and 2D CFD simulations of the Rio Ozama cable-stayed metro railway bridge in tandem arrangement with Francisco del Rosario Sanchez road truss bridge (see Figure 1). Static and dynamic tests were performed on deck sectional models in 1:20 scale in the Politecnico di Milano wind tunnel facility.

Two different shapes of the new bridge deck section were tested (see Figure 2):

- a traditional bluff shape, defined as section A.
- a more streamlined shape with optimized aerodynamic solutions (embedded rails, rounded trailing edges, enhanced barrier porosity), defined as section B.

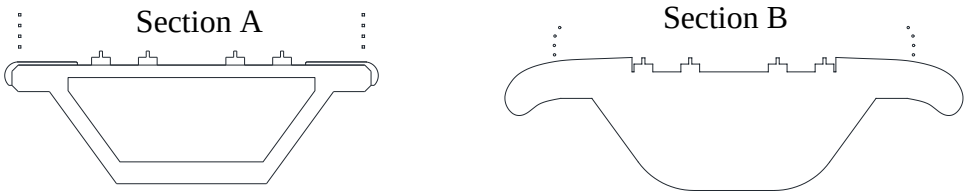

Figure 2. Section A and B: bluff and streamlined version of the deck

The aerodynamic characteristics of the two new bridge solutions were initially investigated in stand alone configuration taking into account that the structure will operate at low reduced velocity, having high natural frequencies, and may suffer of vortex induced vibrations (VIVs).
Once defined the aerodynamic properties in stand alone configuration the aerodynamic interaction with the existing bridge was experimentally and numerically studied by comparing results (both static and dynamic) with the configurations where the new bridge is upwind or downwind the truss bridge. A 2D RANS CFD analysis was conducted to better understand the modifications in the static experimental results induced by the presence of the existing bridge.

2. AERODYNAMICS OF THE TWO SECTIONS AND INTERFERENCE EFFECT OF THE EXISTING BRIDGE

Static and dynamic wind tunnel tests were carried out to measure steady aerodynamic coefficients and direct flutter derivatives for vertical and torsional motion at low reduced velocities with free motion tests. Tests were performed using sectional models, for both section A and B, studying three different scenarios: new deck in stand-alone configuration, upwind the existing deck and downwind. Figure 3 shows a picture taken during the tests.

Figure 3. Pictures of the sectional models in wind tunnel during static and dynamic tests

Sections A and B show a very different aerodynamic behaviour, as expected. As an example, Table 1 reports the steady drag coefficient C_D, the derivative of the moment and lift coefficients K_L and K_M, and the sign of the flutter derivatives a_2^* and h_1^*, at 0 deg angle of attack, in the range of operational reduced velocities. Comparing the two sections, the drag coefficient of section A is twice or more than the one of section B. Moreover, for both sections, C_D in stand-alone configuration is the largest and it is minimum in downwind configuration due to interference effects with the existing bridge.

In stand-alone configuration, the K_L and K_M coefficients are positive and large for section B, as expected, while for section A they have negative values. This is not a good aerodynamic characteristic since, following the quasi-steady approach, it may lead to torsional or vertical 1-dof instabilities. In upwind configuration the K_M coefficients do not change significantly, but the K_L coefficients have both a negative offset with respect to the stand-alone configuration. In downwind, on the contrary, the offset is largely positive and both sections have the $K_L>0$, while the K_M still do not change significantly.

Table 1. Aerodynamic coefficients for sections A and B

	Section A		
	stand alone	upwind	downwind
K_L	-1.6	-2	1.3
K_M	-0.1	0	0
C_D	0.5	0.4	0.26
h_1*		<0	>0
a_2*		<0	0

	Section B		
	stand alone	upwind	downwind
K_L	4.6	3.9	6.5
K_M	1.7	1.6	2
C_D	0.22	0.16	0.14
h_1*		>0	>0
a_2*		>0	>0

The unsteady aerodynamic coefficients at low reduced velocity, measured with free motion tests, follow the behaviour highlighted by the quasi-steady theory. As an example, the direct aeroelastic damping term for the vertical motion h_1^* tends to the value of K_L at high reduced velocities $V^* = V/(fB)$. According to the formulation in Eq.(1) a positive value of h_1^* (or of K_L) indicates a positive aerodynamic damping, therefore it is preferable to design aerodynamic sections with a positive K_L because it is an indicator of the aerodynamic performances of the section at low reduced velocities (that usually are the in service condition of the bridge). As an example the h_1^* coefficients for Sections A and B in upwind and downwind configuration are reported in Figure 4, and they can be compared with steady values reported in Table 1.

$$L = -\left(\frac{1}{2}\rho V^2 B\right) h_1^*\left(\frac{\dot{z}}{V}\right) \tag{1}$$

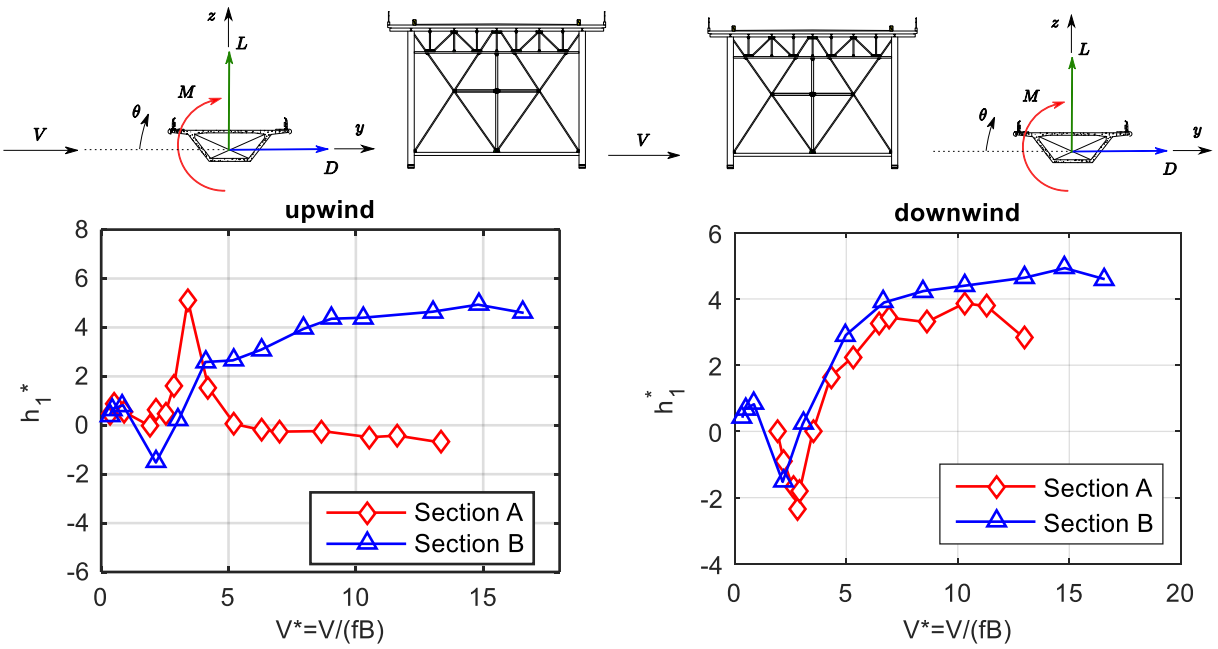

Figure 4. h_1^* aerodynamic coefficient as a function of V^* at mean angle of attack $\alpha = 0$ deg for upwind and downwind configuration

These unsteady aerodynamic coefficients together with the structural characteristics of the bridge allow the designer to assess the critical speed for stability, using a 1-dof approach. As an example, considering the bridge with:

- Deck chord $B = 12$ m
- Effective modal mass per unit length $m = 24600$ kg/m
- Structural damping coefficient $\zeta = 0.004$
- Frequency of the first vertical mode $f_z = 0.54$ Hz

The Scruton number for the vertical mode is

$$Sc_z = 4\frac{m\zeta_z}{\rho B^2} = 2.23 \tag{2}$$

Considering a mean wind velocity at deck height up to 85 m/s, the range of reduced velocities that must be studied is $V^* \leq 13.6$. The stability conditions for 1-dof instability is:

$$Sc_z > -V^* h_1^* / (2\pi) \quad (3)$$

For the vertical motion the instability onset occurs at $V^* = 13.8$. This reduced velocity corresponds to a mean wind speed at deck height of $V = V^* f_z B = 90\ m/s$.

4. CFD ANALYSIS

To furtherly study the results obtained during wind tunnel static tests, a CFD analysis was conducted with the open-source code OpenFOAM®. A 2D low-Re (with wall-functions) URANS approach combined with the k-Ω SST turbulence model, and a fully structured grid was adopted. An initial convergence analysis was conducted, using the experimental results as target values, to verify mesh independency and the effects of surface roughness and Reynolds number. An Equivalent Porosity model was used to model the existing bridge: the truss structure was substituted by groups of cells in which N-S source terms were introduced and calculated according to the Darcy-Forchheimer law.

In particular, CFD simulations were used to instigate the following experimental results:

1. Comparison of Section A and B performances in stand-alone configuration, with a focus on C_D, K_L, and K_M values.
2. Change of sign of K_L (from negative to positive) when Section A is in Downwind Configuration

3.1. Comparison of Section A and B in Stand Alone configuration

3.1.1. Section A

For Section A, the diagram on the left of Figure 5 shows the comparison of pressure coefficients between a positive (+2 deg) and a negative (-2 deg) angle of attack: the difference of the vertical components of the pressure coefficients reported on the right allows one to assess the zones of the deck that lead to a negative K_L.

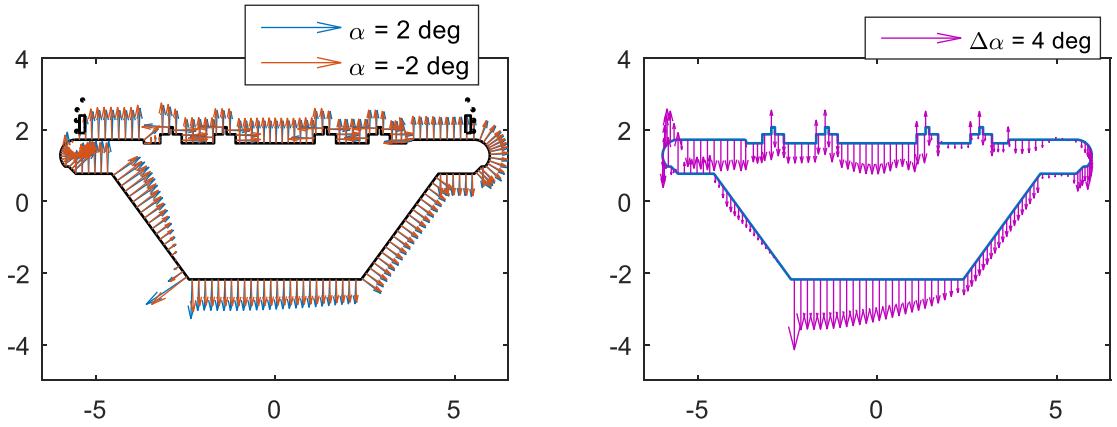

Figure 5. Left: distribution of pressure coefficients for +2 and -2 angle of attack. Right: vertical component of difference between the pressure coefficients multiplied by 10;

Table 2. Contribution of different zones to the global coefficient: Section A stand alone

Zone	K_L	K_L %	K_M
1	-0.60	**36%**	-0.04
2	-0.63	**38%**	-0.02
3	-0.09	6%	0.01
4	-0.21	12%	0.01
5	-0.06	4%	0.02
6	-0.08	5%	0.02
total	-1.68	100%	-0.01

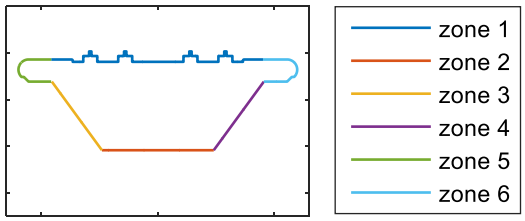

In fact, it is possible to see that the upper and lower surfaces both give a major negative contribution to the KL coefficient. The different contributions are reported in Table 2: the total KL is -1.68 versus an experimental value of -1.6. As far as the K_M is concerned, both experimental and numerical values are about zero: the negative contributions of the zone 1 and 2 are in fact compensated by the contributions of the other zones of the deck.

3.1.1. Section B

For Section B, the diagram on the left of Figure 6 shows the comparison of pressure coefficients between a positive (+2 deg) and a negative (-2 deg) angle of attack: the difference of the vertical components of the pressure coefficients reported on the right allows one to assess the zones of the deck that lead to positive K_L and K_M.

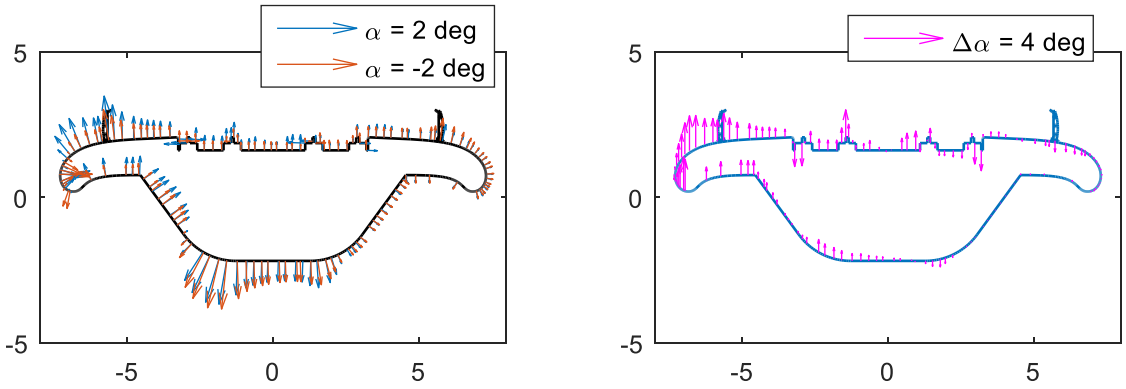

Figure 6. Left: distribution of pressure coefficients for +2 and -2 angle of attack. Right: vertical component of difference between the pressure coefficients multiplied by 2

Table 3. Contribution of different zones to the global coefficient: Section B stand alone

Zone	K_L	K_L %	K_M	K_M %
1	1.21	**30%**	0.14	9%
2	0.25	6%	0.04	3%
3	0.42	11%	0.12	8%
4	-0.01	0%	-0.01	-1%
5	2.41	**61%**	1.14	**73%**
6	-0.30	-8%	0.13	8%
total	4	100%	1.6	100%

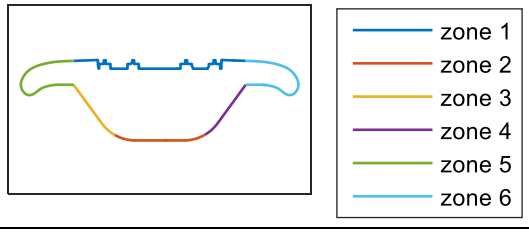

In this case, the major contribution to the positive values is due to the upwind nose of deck (zone 5), as it is highlighted in Table 3. The numerical K_L is 4 versus an experimental one of 4.6, while the numerical K_M is 1.6 versus an experimental one of 1.7.

Figure 7 shows a qualitative comparison of the flow velocity fields, where it is possible to see that the smooth shape and the embedded rails of Section B reduce the dimension of the wake and the region of separated flow especially in the upper and lower surface.

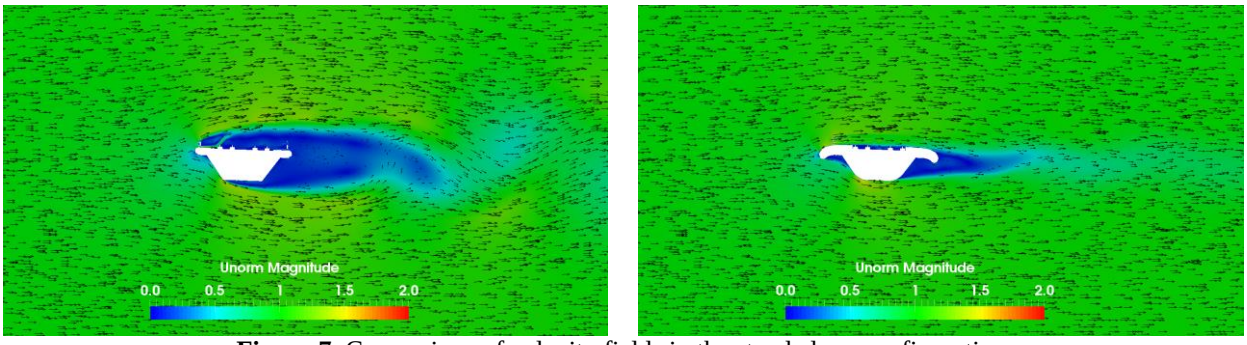

Figure 7. Comparison of velocity fields in the stand alone configurations

3.1. Change of sign of K_L in downwind configuration for Section A

Similar analyses can be performed to study the change of sign in the lift coefficient for the downwind configuration of Section A. The diagram on the left of Figure 8 shows the comparison of pressure coefficients between a positive (+2 deg) and a negative (-2 deg) angle of attack in downwind configuration: the difference of the vertical components of the pressure coefficients reported on the right allows one to assess the zones of the deck that lead to a change of sign in the K_L.

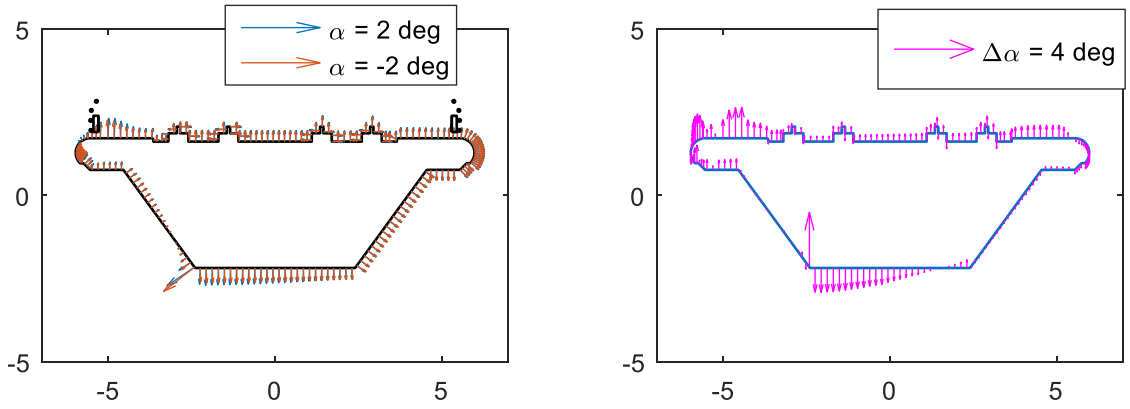

Figure 8. Left: distribution of pressure coefficients for +2 and -2 angle of attack. Right: vertical component of difference between the pressure coefficients multiplied by 10

Table 4. Contribution of different zones to the global coefficient: Section A downwind

Zone	K_L	K_L %	K_M
1	0.35	**61%**	-0.05
2	-0.20	**-35%**	-0.02
3	0.01	1%	0.01
4	0.01	2%	-0.02
5	0.29	**50%**	0.12
6	0.12	21%	-0.07
total	0.58	100%	-0.02

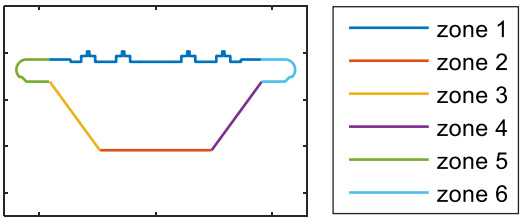

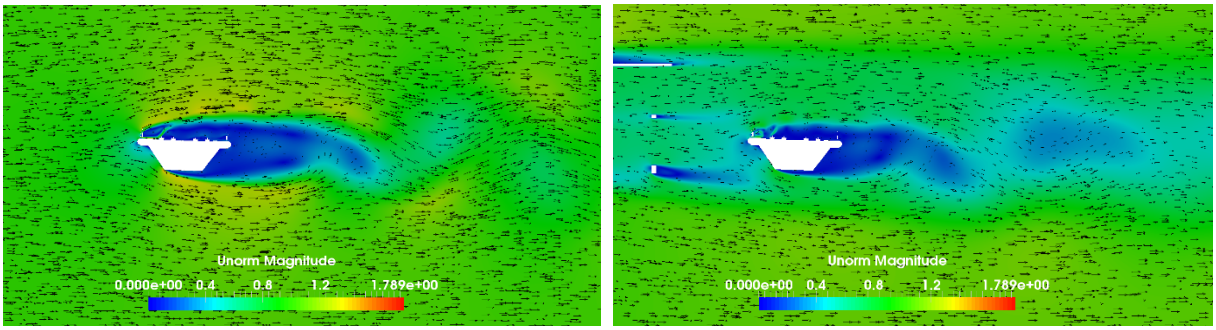

Figure 9. Comparison of velocity fields in the stand alone versus downwind configurations

It is possible to notice that in comparison with the stand alone configuration the upper surfaces now generate a positive contribution. This is shown in Table 4, where it is reported that zones 1 and 5 play a major role in the K_L value. The numerical K_L is 0.58 versus an experimental value of 1.3: the discrepancy can be related to the simplistic modelling of the upwind bridge interference effect (that was modelled by means of an equivalent porosity). Nevertheless, the change in the slope is simulated, and it is expected that the flow pattern is close to the experimental one. Figure 9 shows that the deck is in the wake of the upwind bridge and the relative position between the two bridges determines the interference between the wake of the truss elements and the deck.

5. CONCLUSIONS

The aerodynamic interaction effects between decks in tandem arrangement were investigated by means of wind tunnel tests and CFD simulations.

In the considered case the aerodynamic interaction can cause a significant change in the slopes of the static coefficients, even producing a sign change. This could affect the aerodynamic stability of the bridges: even if for the specific case the assessment of the stability has to consider low reduced velocities, the quasi-steady values are an indicator of the unsteady behaviour of the deck. 2D CFD simulations helped to compare the pressure distributions and the flow field for different sections and configurations, explaining the major interaction mechanism that led to a change in the coefficients for the bluff deck with a sharp-edge section, and the more performing aerodynamic behaviour of the mode streamlined deck, with smooth edges and embedded rails, which is less sensitive to the tandem arrangement interaction.

REFERENCES

Argentini, T., Rocchi, D., Zasso, A., 2015. Aerodynamic interference and vortex-induced vibrations on parallel bridges: The Ewijk bridge during different stages of refurbishment. Journal of Wind Engineering and Industrial Aerodynamics. Volume 147, Pages 276–282.

Seo, J.-W.; Kim, H.-K.; Park, J.; Kim, K.-T. & Kim, G.-N., 2013. Interference effect on vortex-induced vibration in a parallel twin cable-stayed bridge. Journal of Wind Engineering and Industrial Aerodynamics, 116, 7-20

Meng, X.; Zhu, L. & Guo, Z., 2011. Aerodynamic interference effects and mitigation measures on vortex-induced vibrations of two adjacent cable-stayed bridges. Frontiers of Architecture and Civil Engineering in China, 5, 510-517

Larsen, S. V.; Astiz, M. A. & Larose, G. L., 2000. Aerodynamic Interference Between Two Closely Scaced Cable Supported Bridges. Fourth International Colloquium on Bluff Body Aerodynamics and Applications, 33-37

Kimura, K.; Shima, K.; Sano, K.; Kubo, Y.; Kato, K. & Ukon, H., 2008. Effects of separation distance on wind-induced response of parallel box girders. Journal of Wind Engineering and Industrial Aerodynamics, 2008, 96, 954-962